Journal of Alloys and Compounds 526 (2012) 119–124

Contents lists available at SciVerse ScienceDirect

# Journal of Alloys and Compounds

journal homepage: www.elsevier.com/locate/jallcom

# Influence of the GaN spacer thickness on the structural and photoluminescence properties of multi-stack InN/GaN quantum dots

Wen-Cheng Ke[a,*], Shuo-Jen Lee[a], Shiow-Long Chen[a], Chia-Yu Kao[a], Wei-Chung Houng[a], Chih-An Wei[a], Yi-Ru Su[b]

[a] *Department of Mechanical Engineering, Yuan Ze University, Chung-Li 320, Taiwan, ROC*
[b] *Department of Photonics Engineering, Yuan Ze University, Chung-Li 320, Taiwan, ROC*

ARTICLE INFO

*Article history:*
Received 27 September 2011
Received in revised form 11 January 2012
Accepted 31 January 2012
Available online xxx

*Keywords:*
InN QDs
GaN capping
Photoluminescence
Strain

ABSTRACT

This paper reports the structural and photoluminescence (PL) characteristics of single-layer and multi-stack InN/GaN quantum dots (QDs) with varying spacer thickness. A single crystalline 10-nm thick GaN capping layer is grown on the InN QDs by the flow-rate modulation epitaxy (FME) method. The PL peak is red shifted down to 18 meV and its full width at half maximum (FWHM) was narrowed from 104 meV to 77 meV as increasing GaN capping layer thickness to 20-nm. The red-shift and the linewidth narrowing of the PL spectra for the single-layer InN QDs as a result of the increase in capping thickness are believed to be due to the fact that the GaN capping layer decreases the surface defect density thereby decreasing the surface electron concentration of the InN QDs. However, the PL intensity decreases rapidly with the increase in GaN spacer thickness for the three-layer stacked InN/GaN QDs. Because of kinetic roughening, the 20-nm thick GaN capping layer shows a roughened surface. This roughened GaN capping layer degrades the InN QDs growth in the next layer of multi-stack InN QDs. In addition, the increased compressive strain on the InN QDs with the increase in GaN spacer thickness increases the defect density at the InN/GaN capped interface and will further decrease the PL intensity. After the GaN spacer thickness is modified, the PL intensity of the three-layer stacked sample with a 10-nm thick GaN spacer layer is about 3 times that of the single-layer sample.

© 2012 Elsevier B.V. All rights reserved.

## 1. Introduction

Revising the InN band gap energy to ∼0.7 eV [1], has promised many additional applications of optoelectronic devices in the infrared range, including high efficiency solar cells. In recent years, the benefits of multiple exciton generation have been demonstrated in colloidal suspensions of PbSe, PbS, PbTe, CdSe, and GaAs QDs by achieving high-efficiency nanostructured solar cells [2,3]. In order to increase the absorption of nanostructured solar cells, it is necessary to increase the volume of the nanostructure. In other words, the growth technique for high density QDs [4,5] or for the stacking the QD layers plays an important role in increasing the density of the dot volume. These findings motivate studying the structural and optical behaviors of the multi-stack InN/GaN QDs structure.

The InN QDs are formed through self-assembly in the highly mismatched InN/GaN system (i.e., with a lattice mismatch of ∼11%) by means of the "Stranski–Krastanov (SK: layer-plus-island)" growth mode [6]. The relaxation of misfit strain was shown to be initiated by formation of misfit dislocations (MDs) at the heterointerface between the InN and GaN [7–9]. The introduction of a low temperature GaN capping layer also induces a rearrangement of the MDs at the InN/GaN capped interface [10]. In addition, due to the thermal instability the low InN dissociation temperature and high equilibrium nitrogen vapor pressure over the InN limits the growth temperature of the GaN capping layer. Generally speaking, low-temperature GaN film has poor crystal quality and a high defect density. The kinetic roughening due to the low Ga adatom surface mobility at low growth temperature increases with the increase in layer thickness. A high-defect density and/or roughened surface of the GaN capping layer acts as a favorable nucleation site that influences the nucleation of QDs in the growth of the next layer of multi-stack InN/GaN QDs. Thus, it is necessary to modify the spacer thickness in order to obtain a high crystal quality and a smooth surface of the GaN spacer layer in the stacked InN/GaN QDs. It is therefore essential that a systemic investigation of the effect of spacer thickness on the structural and optical properties of multi-stack InN/GaN QDs.

## 2. Experimental details

The InN/GaN QDs structures were grown on 1 μm thick GaN/(0 0 0 1) sapphire substrates by low pressure metal organic chemical vapor deposition. The InN QDs were grown by pulsed

* Corresponding author.
*E-mail address:* wcke@saturn.yzu.edu.tw (W.-C. Ke).

0925-8388/$ – see front matter © 2012 Elsevier B.V. All rights reserved.
doi:10.1016/j.jallcom.2012.01.158

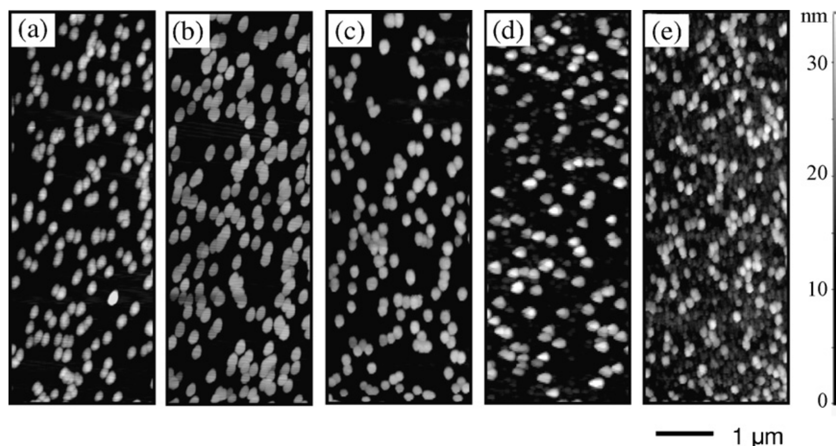


**Fig. 1.** AFM images of (a) un-capped InN QDs, single-layer InN QDs covered by (b) a 10-nm thick and (c) a 20-nm thick GaN capping layer, and three-layer InN QDs with (d) a 10-nm thick GaN spacer, and (e) a 20-nm thick GaN spacer.

mode (PM) method at a temperature of 650 °C to achieve higher density. The gas flow sequence for the PM method basically consists of four steps: 20 s TMIn + $NH_3$ growth step, 20 s $NH_3$ source step with 10 s purge steps in between. During the growth step, the mole flow rates of TMIn and $NH_3$ are $1.53 \times 10^1$ and $8.04 \times 10^5$ μmol/min, respectively. The InN QDs layer is then covered by a series of GaN capping layers with a thickness of 10 nm, 15 nm or 20 nm at 650 °C respectively, using the FME method, respectively. The mole flow rates of TMGa and $NH_3$ are $2.21 \times 10^1$ μmol/min and $1.79 \times 10^5$ μmol/min, respectively for FME growth of GaN capping layer. The same InN/GaN bilayer is then deposited two more times such that a stacked structure is created comprising of three InN QDs planes separated by three GaN barriers. The PL measurements are performed using the 488-nm line of an argon-ion laser as the excitation source. The PL signals are dispersed by an ARC Pro 500 monochromator and are detected by a cooled InGaAs photodiode with a cutoff wavelength of 2.05 μm.

## 3. Results and discussion

Fig. 1 shows the atomic force microscopy (AFM) images of the uncapped InN QDs, the single-layer and the three-layer InN QDs. The QDs density is $\sim 1.5 \times 10^9$ cm$^{-2}$ for both the uncapped InN QDs and single-layer InN QDs. The GaN capping morphology plays an important role in achieving a well stacked multilayered structure. The flat surface and high quality of the GaN capping layer is helpful for achieving high PL intensity of multi-stack InN QDs. In Fig. 1(c) and (d), the root mean square (RMS) surface roughness are 0.542 nm and 1.284 nm respectively for 10-nm thick and 20-nm-thick GaN capping layer. The AFM line scan profiles indicated that the surface morphology of the 10-nm thick GaN capping layer shows a truncated pyramid shape and changes to a dome shape when the thickness of the capping layer increases to 20-nm. In Fig. 1(d), the QDs density remains at $\sim 1.5 \times 10^9$ cm$^{-2}$ for the three-layer InN QDs with a 10-nm thick GaN spacer layer. However, the QDs density increases to $2.1 \times 10^9$ cm$^{-2}$ when the spacer thickness increases to 20 nm (see Fig. 1(e)). Additionally, the size of the InN QDs for the three-layer samples shows a decreasing trend with the increase in thickness of the GaN spacer. The density and size of the InN QDs depend not only on the stacking layer but also on the thickness of the spacer.

The transmission electron microscopy (TEM) images shown in Fig. 2 were used to study the structural properties of the uncapped InN QDs, and of the single-layer samples. The insert in Fig. 2(a), shows the atomically sharp and flat 3 monolayers (MLs)-thick InN wetting layer on the GaN layer. The critical thickness for the SK mode forming InN QDs is about ~0.86 nm. In comparison with Fig. 2(b) and (c), the surface morphology of the 10-nm thick GaN capping is smooth, changing to a rough surface when the capping thickness increases to 20-nm. The surface roughness of GaN capping layer evidence from these TEM images in agreement with AFM observations. Fig. 2(d) shows that a smooth and single crystalline GaN capping layer can be grown on the InN QDs by FME method to increase the migration length of the Ga adatoms at the lower growth temperature. However, because the kinetic roughening becomes greater as the layer thickness increases, the 20-nm thick GaN capping layer shows a roughened surface. This rough GaN capping surface will form more favorable nucleation sites to increase the QDs density but decrease the size of InN QDs growth in the next layer, since the total amount of InN deposited is the same. Thus, the dot size of the three-layer samples shows a decreasing trend with the increase in GaN spacer thickness (see Fig. 1(d) and (e)).

In order to study the strain level in the multi-stacked InN QDs, we performed an X-ray diffraction (XRD) measurement. Fig. 3(a) shows the (0 0 2) $\omega/2\theta$ scans of the uncapped InN QDs, the single-layer and the three-layer InN QDs. Combining Bragg's law with the expression for the inter-planar spacing in hexagonal structures, the lattice constant in the growth direction is found to be $c = l \times \lambda/(2\sin\theta_B)$, for any allowed (0 0 l) reflection of X-rays of the wavelength $\lambda$. For this calculation, the lattice constant ($c$ axis) of the GaN buffer layer is 5.185 Å, and the lattice constant ($c$ axis) of the uncapped InN QDs is 5.717 Å. The values of the lattice constants for the case of stain-free InN are estimated to be in the range of $c$ = 5.703 Å [11]. The larger lattice constant, $c$, is attributed to the uniaxial tensile stress in the growth direction of the uncapped InN QDs. In contrast, the lattice constant is 5.689 Å for InN QDs covered by a 20-nm thick GaN capping layer. Fig. 3(b) shows the reduction of the lattice constant with a capping thickness for a single-layer sample indicating that the GaN capping process exerts a compressive strain on the InN QDs. In addition, the residual strain relaxation in the InN dots with different thickness of GaN capping layer were also studied. The strain ($\varepsilon_{zz}$) along $z$ axis was estimated from the relation

$$\varepsilon_{zz} = \frac{C - C_0}{C_0} \times 100\% \tag{1}$$

where $C$ denotes the lattice constant of the InN dots and $C_0$ is strain-free InN films. The residual strain is reduced from 0.245% to 0.07% as the GaN cap thickness increased from 0 to 10 nm. However, the residual strain of InN dots reduced to −0.245% for 20-nm thick GaN

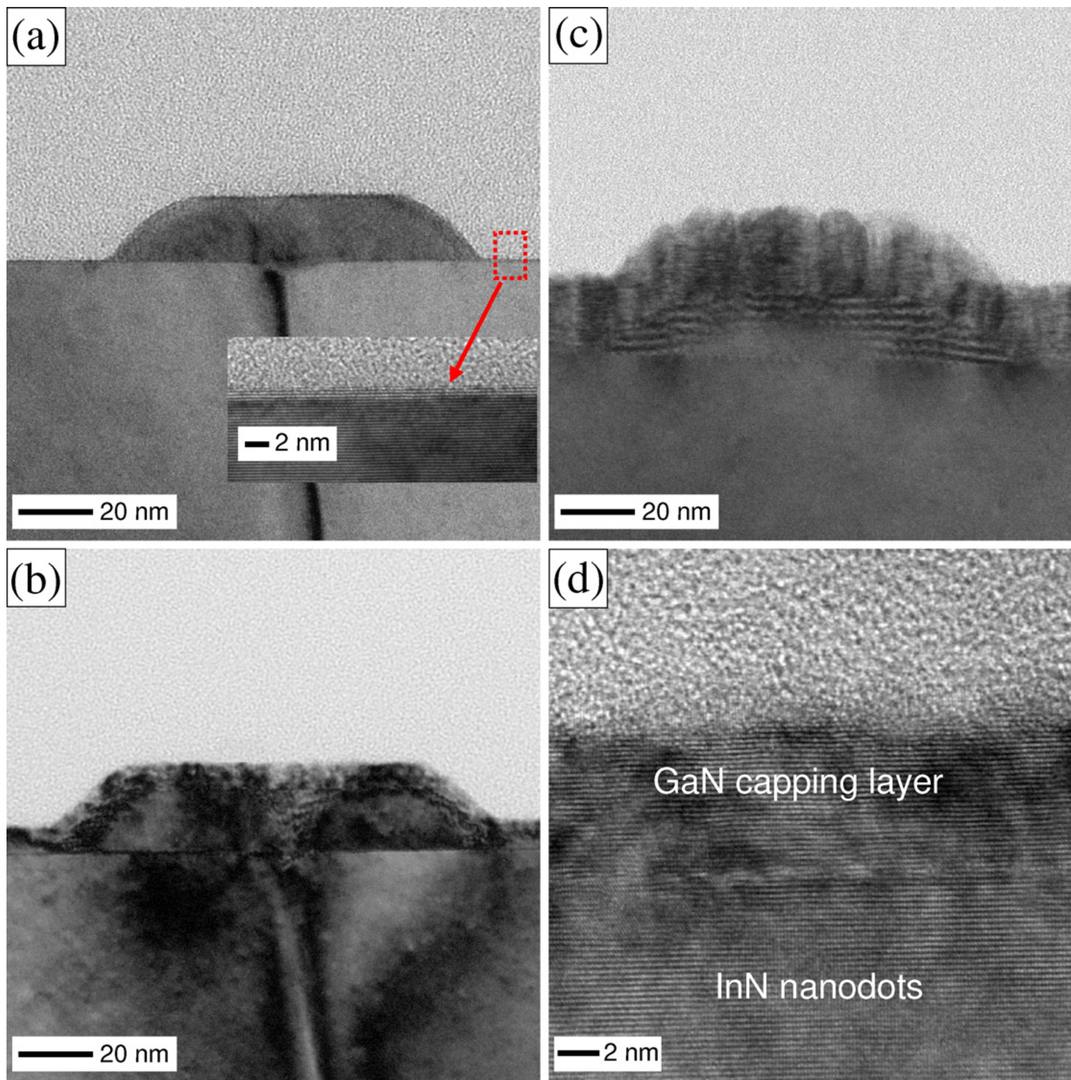


**Fig. 2.** TEM images of (a) un-capped InN QDs, single-layer InN QDs covered by (b) a 10-nm thick GaN capping layer, and (c) a 20-nm thick GaN capping layer. The inset in (a) shows the HRTEM image of the InN wetting layer on the GaN films, and (d) the HRTEM image of InN QDs covered by a 10-nm thick GaN capping layer.

capping layer. We also used Scherrer's equation [12] to calculate the size of the InN QDs as follows.

$$\beta \cdot \cos\ \theta_B = \frac{k\lambda}{d} \tag{2}$$

where $\beta$ is the full width at half maximum (FWHM) values of (0 0 2) XRD peak, and $d$ denotes the height of the InN QDs. Constant $k$ is 0.8, and $\lambda$ denotes the wavelength of the incident X-ray. In Fig. 3(c), the height of the dots for the three-layer samples shows a decreasing trend with the increase in GaN spacer thickness. It should be noted that a double peak is found for the three-layer sample with a 20-nm thick GaN spacer layer, indicating the dot size non-uniformity in the multi-stack InN/GaN QDs.

Fig. 4 shows the 17K-PL spectra of the un-capped InN QDs, as well as the single-layer and three-layer InN QDs with various GaN spacer thicknesses. Note that the PL of the sample with 20-nm-thick GaN spacer is too weak to be measured. The Gaussian fitting of the PL spectrum for uncapped InN QDs shows a peak energy at 0.807 eV, with a FHWM of 104 meV. The PL peak energy red shifted to a lower energy of 0.789 eV with increasing GaN capping layer thickness to 20-nm. In addition, the PL FWHM can be decreased to 77 meV by increasing of GaN capping thickness to 20-nm. In order to understand the changes in PL peak energy with the increase in GaN capping thickness, we assume that the InN QDs bandgap energy (i.e. $E_g$) is 0.7 eV, we take the strain effect (i.e. $\Delta E_g^{st}$) [13] and the piezoelectric effect (i.e. $\Delta E_g^{QCSE}$) [13] as well as the quantum confinement effect (i.e. $\Delta E_{conf.}$) [14], and calculate the electron Fermi energy (i.e. $\Delta E_F(n_e)$) [15,16] which is determined by the residual electron concentration in the InN QDs.

The total change in band gap due to strain could be estimated as sum of the contributions from change in conduction and valance bands (heavy hole), as in Eq. (3)

$$\Delta E_g^{st} = \Delta E_c^{st} - \Delta E_{v,hh}^{st} \tag{3}$$

The change in conduction band due to strain is calculated [17,18] as:

$$\Delta E_c^{st} = a_c^z \left(-\frac{2C_{13}}{C_{33}}\Delta\varepsilon_{xx}\right) + a_c^{x,y}(2\Delta\varepsilon_{xx}) \tag{4}$$

where $a_c^z$ and $a_c^{x,y}$ are hydrostatic deformation potential constants.

The calculation [18,19] of valance band shift due to strain is as follows:

$$\Delta E_{v,hh}^{st} = [D_1\Delta\varepsilon_{zz} + D_2(\Delta\varepsilon_{xx} + \Delta\varepsilon_{yy})] + [D_3\Delta\varepsilon_{zz} + D_4(\Delta\varepsilon_{xx} + \Delta\varepsilon_{yy})] \tag{5}$$

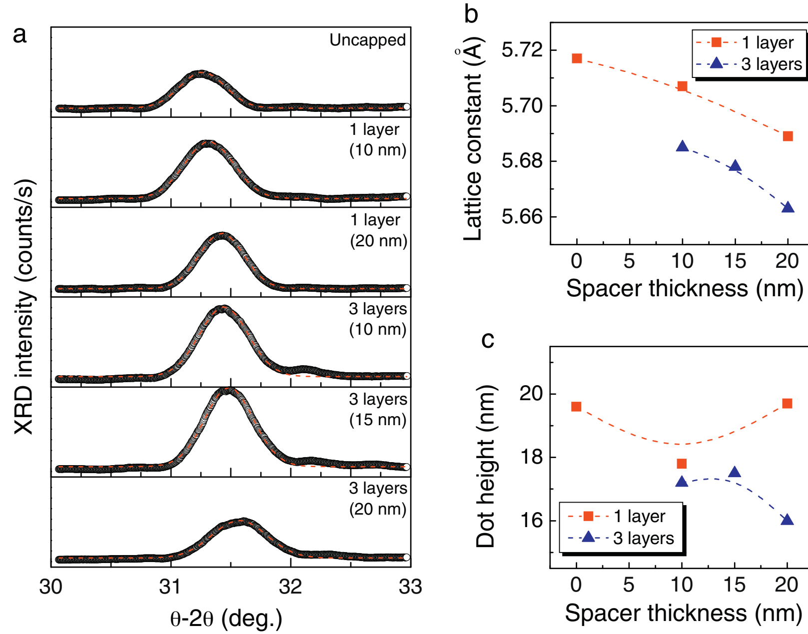


**Fig. 3.** (a) The (0 0 2) XRD measurement of un-capped, single-layer and three-layer InN QDs with various GaN spacer thickness. The red color of the dashed line is the Gaussian fitting curve. (b) The relationship between lattice constant and GaN spacer thickness. (c) The relationship between dot height and GaN spacer thickness. (For interpretation of the references to color in figure legend, the reader is referred to the web version of the article.)

The change in the band gap due to electric field, quantum-confinement Stark effect (QCSE), could be approximated as [20]:

$$\Delta E_g^{QCSE} = \frac{C_1(m_e^* + m_h^*)m_0 e^2 \varepsilon^2 L^4}{\hbar^2} \quad (6)$$

where $C_1 = -2.19 \times 10^{-3}$, $L$ is InN QDs height, $m_0$ is the electron mass, and $e$ is the unit charge.

Based on the effective mass theory, the band gap enhancement $\Delta E_{conf.}$ for low-dimensionally confined InN QDs can be estimated as [14]:

$$\Delta E_{conf.} \approx \frac{\pi^2\hbar^2}{2d^2}\left(\frac{1}{m_e^*} + \frac{1}{m_h^*}\right) \quad (7)$$

where $\hbar$, $m_e^* = 0.07m_0$, $m_h^* = 0.1m_0$ are Planck's constant and the effective masses of an electron and a hole, respectively.

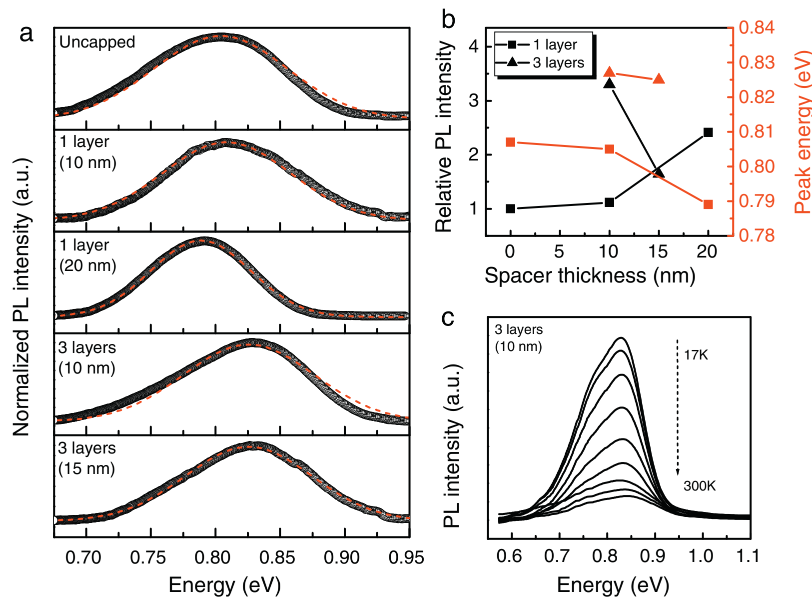


**Fig. 4.** (a) The 17K PL spectra of un-capped, single-layer and three-layer InN QDs with various GaN spacer thickness. The red color of the dashed line is the Gaussian fitting curve. (b) The relationship between PL intensity/peak energy and GaN spacer thickness. (c) The temperature dependent PL measurement of three-layer InN QDs with a 10-nm thick GaN spacer. (For interpretation of the references to color in figure legend, the reader is referred to the web version of the article.)

**Table 1**
The calculated results of the confinement effect and the Fermi energy for the samples of this study. The dot height for the different samples are shown for comparison.

| | QDs height (nm) | $E_{PL}$ (eV) | $\Delta E_{conf.}$ (meV) | $\Delta E_F(n_e)$ (meV) | $n_e$ (cm$^{-3}$) |
|---|---|---|---|---|---|
| Uncapped | 19.6 | 0.807 | 33.3 | 77.4 | $1.84 \times 10^{18}$ |
| 1 layer (10 nm) | 17.8 | 0.804 | 39.9 | 76.5 | $1.79 \times 10^{18}$ |
| 1 layer (20 nm) | 19.7 | 0.789 | 32.6 | 56.4 | $1.14 \times 10^{18}$ |
| 3 layers (10 nm) | 17.2 | 0.827 | 43.0 | 83.9 | $2.07 \times 10^{18}$ |
| 3 layers (15 nm) | 17.5 | 0.825 | 41.6 | 85.4 | $2.12 \times 10^{18}$ |

The Burstein–Moss shift of the Fermi energy $\Delta E_F(n_e)$ is expressed as follows [16]:

$$\Delta E_F(n_e) = 3.62 \times 10^{-3} \left(\frac{m_0}{m_e^*}\right) (n_e \times 10^{-24})^{2/3} \quad (8)$$

The calculation of the strain effect on the InN/GaN dots band gap is in the order of several meV, and is not the dominant effect on the PL peak energy. Due to the large height of the InN QDs, the change in bandgap via electric field, quantum-confined Stark effect, is in the order of several eV, which is not reasonable in these samples. Since the height/width of uncapped InN QDs is 19.6/103 nm, the quantum confinement effect induced confinement energy is about ~33.3 meV. Cimalla et al. showed that the high surface electron concentration generated by the high surface density of states is due to the high ratio of surface area to the volume of nanodots [21]. It is well known that the thermal instability is due to the low InN dissociation temperature and high equilibrium $N_2$ vapor pressure over the InN implies nitrogen desorption from the dots. We believe that GaN capping avoids InN decomposition and decreases the surface defect density. The high resolution TEM (HRTEM) image shows the sharp interface between the InN QDs and the GaN capping layer (see Fig. 2(d)). The surface lattice imperfection of the uncapped InN QDs (not shown here) can be repaired by the capping process. The GaN capping decreases the surface defect density and therefore decreases the surface electron concentration of the InN QDs. Thus, the PL peak energy can be roughly estimated by $E_{PL} \approx E_g + \Delta E_{conf.} + \Delta E_F(n_e)$ in these samples. The calculated results are summarized in Table 1. The decrease in PL peak energy and the FWHM for the single-layer InN QDs can be well explained by the optimal GaN capping process.

Fig. 4 shows that the PL peak energy of the three-layer samples is higher than that of the single-layer sample with a 10-nm thick GaN spacer. The electron concentration is estimated to increase from $1.79 \times 10^{18}$ cm$^{-3}$ to $2.07 \times 10^{18}$ cm$^{-3}$. It has been reported that the GaN capping layer is fully relaxed by the introduction of a misfit dislocation (MD) network, while the dots increase the residual strain [10]. Thus, it can be realized that there is a higher electron concentration in the three-layer InN QDs than in the single-layer sample. Fig. 3(c) shows that the average height of three-layer InN QDs with 10-nm thick spacer layer is 17.2 nm, which is smaller than the 17.8 nm of the single-layer InN QDs covering a 10-nm thick capping layer. We believe that the quantum size effect also contributes to the blue-shift of the PL spectra. In Fig. 4(b), it must be noted that the increase in GaN spacer thickness to 15-nm for three-layer samples results in a decrease in the PL intensity, since the generation of MDs during epitaxial growth is gradual, depending on the thickness of the capping layer [10]. In Fig. 3(b), the lattice constant decreases with the increase in spacer thickness for the three-layer samples, indicating that more compressive strain is being exerted on the InN QDs. Thus, more MDs are formed at the interface between the GaN spacer and InN QDs in order to balance the stress between the layers. This decrease in PL intensity may be due to the fact that the thicker GaN spacer induces a high density non-radiation center such as misfit dislocation between the InN QDs and the GaN spacer. In this study, the optimal spacer thickness is 10-nm for the stacked InN/GaN multilayer QDs. The PL intensity of the 10-nm-thick GaN spacer of the three-layer sample increases about 3-fold, compared with that of the single-layer sample. The experimental results indicated that the PL intensity of multi-stack InN QDs is not only dependent on the stacking layer but also on the spacer thickness. Controlling GaN spacer thickness to obtain high crystal quality and smooth surface of GaN spacer layer are critical points for achieving a well multi-stack InN/GaN QDs structures.

Finally, we measure the temperature dependent PL of the three-layer InN QDs with a 10-nm thick GaN spacer. Fig. 4(c) shows that the measured PL peak energy increases with the increase in temperature. This phenomenon is explained by the higher surface electron concentration of the InN QDs, generated by the high surface density of state, having a tendency to substantially increase when the temperature increases [4]. The number of trapped surface electrons that become thermally excited to the conduction band increases substantially. This then of course results in an increase of the Fermi energy and subsequently a higher measured temperature for the blue-shifted PL energy of the emitted photons. The carrier localization effect of the InN QDs is further investigated using reduced thermal quenching of the PL from the QDs. The thermal activation energy is estimated to be ~74 meV, indicating a strong localization effect in the multi-stack InN/GaN QDs.

## 4. Conclusion

In summary, a single crystalline and smooth surface of 10-nm thick GaN capping layer is successfully grown on the InN QDs by FME method at 650 °C. The TEM and PL results indicated that the high crystal quality GaN capping layer decreases the surface defect density and therefore decreases the surface electron concentration of the InN QDs. However, the surface morphology of GaN capping layer becomes rough when the thickness increases to 20-nm. The roughened GaN capping layer then degrades the InN QDs growth in the next layer of multi-stack InN QDs. In addition, the increased compressive strain on the InN QDs due to the increased GaN spacer thickness will increase the defect density at the InN/GaN interface. The surface morphology and thickness of GaN spacer layer play important roles for achieved high PL intensity of the multi-stack InN/GaN QDs structures.

## Acknowledgement

The authors gratefully acknowledge the financial support from the National Science Council of Taiwan, ROC under Contract No. NSC-98-2112-M155-001-MY3.

## References

[1] J. Wu, W. Walukiewicz, K.M. Yu, J.W. Ager III, E.E. Haller, H. Lu, W.J. Schaff, Y. Saito, Y. Nanishi, Appl. Phys. Lett. 80 (2002) 3967.
[2] O. Jani, I. Ferguson, C. Honsberg, S. Kurtz, Appl. Phys. Lett. 91 (2007) 132117.
[3] C.J. Neufeld, N.G. Toledo, S.C. Cruz, M. Iza, S.P. DenBaars, U.K. Mishra, Appl. Phys. Lett. 93 (2007) 143502.
[4] W.C. Ke, S.J. Lee, C.Y. Kao, W.K. Chen, W.C. Chou, M.C. Lee, W.H. Chang, W.J. Lin, Y.C. Cheng, T.C. Lee, J.C. Lin, J. Cryst. Growth 312 (2010) 3209.
[5] S. Ruffenach, O. Briot, M. Moret, B. Gil, Appl. Phys. Lett. 90 (2007) 153102.
[6] A. Yoshikawa, N. Hashimoto, N. Kikukawa, S.B. Che, Y. Ishitani, Appl. Phys. Lett. 86 (2005) 153115.
[7] S. Srinivasan, L. Geng, R. Liu, F.A. Ponce, Y. Narukawa, S. Tanaka, Appl. Phys. Lett. 83 (2003) 5187.

[8] Th. Kehagias, A. Delimitis, Ph Komninou, E. Iliopoulos, E. Dimakis, A. Georgakilas, G. Nouet, Appl. Phys. Lett. 86 (2005) 151905.
[9] C.J. Lu, X.F. Duan, H. Lu, W.J. Schaff, J. Mater. Res. 21 (2006) 1693.
[10] J.G. Lozano, A.M. Sánchez, R. García, D. González, M. Herrera, N.D. Browning, S. Ruffenach, O. Briot, Appl. Phys. Lett. 92 (2008) 231907.
[11] I. Vurgaftman, J.R. Meyer, J. Appl. Phys. 94 (2003) 3675.
[12] C.V. Ramana, R.S. Vemuri, I. Fernandez, A.L. Campbell, Appl. Phys. Lett. 95 (2009) 231905.
[13] C. Bayram, M. Razeghi, Appl. Phys. A 96 (2009) 403.
[14] W.C. Ke, C.P. Fu, C.Y. Chen, L. Lee, C.S. Ku, W.C. Chou, W.-H. Chang, M.C. Lee, W.K. Chen, W.J. Lin, Y.C. Cheng, Appl. Phys. Lett. 88 (2006) 191913.
[15] W.-H. Chang, W.-C. Ke, S.-H. Yu, L. Lee, C.-Y. Chen, W.-C. Tsai, H. Lin, W.-C. Chou, M.-C. Lee, W.-K. Chen, J. Appl. Phys. 103 (2003) 104306.
[16] T. Inushima, T. Sakon, M. Motokawa, J. Cryst. Growth 269 (2004) 173.
[17] M. Grundmann, O. Stier, D. Bimberg, Phys. Rev. B 52 (1995) 11969.
[18] C.G. Van de Walle, M.D. McCluskey, C.P. Master, L.T. Romano, N.M. Johnson, Mater. Sci. Eng. B 59 (1999) 274.
[19] S.L. Chuang, C.S. Chang, Phys. Rev. B 54 2491 (1996).
[20] S.L. Chuang, Physics of optoelectronic devices, Wiley, New York, 1995.
[21] V. Cimalla, V. Lebedev, F.M. Morales, R. Goldhahn, O. Ambacher, Appl. Phys. Lett. 89 (2006) 172109.